Direct Observation of Decoupled Structural and Electronic Transitions and an Ambient Pressure Monocliniclike Metallic Phase of VO_{2}

J. Laverock, S. Kittiwatanakul, A. A. Zakharov, Y. R. Niu, B. Chen, S. A. Wolf, J. W. Lu, and K. E. Smith

Direct Observation of Decoupled Structural and Electronic Transitions and an Ambient Pressure Monoclinic-Like Metallic Phase of VO$_2$

J. Laverock,[1] S. Kittiwatanakul,[2] A. A. Zakharov,[3] Y. R. Niu,[3] B. Chen,[1] S. A. Wolf,[2, 4] J. W. Lu,[4] and K. E. Smith[1, 5]

[1]*Department of Physics, Boston University, 590 Commonwealth Avenue, Boston, MA 02215, USA*
[2]*Department of Physics, University of Virginia, Charlottesville, VA 22904, USA*
[3]*MAX-lab, Lund University, SE-221 00 Lund, Sweden*
[4]*Department of Materials Science and Engineering,*
University of Virginia, Charlottesville, VA 22904, USA
[5]*School of Chemical Sciences and The MacDiarmid Institute for Advanced Materials and Nanotechnology,*
The University of Auckland, Private Bag 92019, Auckland 1142, New Zealand

We report the simultaneous measurement of the structural and electronic components of the metal-insulator transition of VO$_2$ using electron and photoelectron spectroscopies and microscopies. We show that these evolve over different temperature scales, and are separated by an unusual monoclinic-like metallic phase. Our results provide conclusive evidence that the new monoclinic-like metallic phase, recently identified in high-pressure and nonequilibrium measurements, is accessible in the thermodynamic transition at ambient pressure, and we discuss the implications of these observations on the nature of the MIT in VO$_2$.

The metal-insulator transition (MIT) of VO$_2$ is one of the most intensively studied examples of its kind, and yet it continues to surprise and inform us: some recent examples include the observation of its solid-state triple-point, which is remarkably found to lie at the ambient pressure transition temperature,[1] and the peculiar nano-sized striped topographical pattern that has been found in strained VO$_2$ films.[2,3] Moreover, the phase transition itself faces renewed questions as to its origin and mechanism following the discovery at high pressure, and in nonequilibrium experiments, of a metallic state of monoclinic symmetry,[4–6] which beforehand had universally been the reserve of the insulating state in experiments. Very recently, the decoupling of the structural and electronic phase transitions has been confirmed in the related compound, V$_2$O$_3$.[7] In part, the widespread interest that VO$_2$ has attracted is owed to the accessibility of its sharp,[8] ultrafast[9] transition, occurring in the bulk at 65 °C at ambient pressures, coupled with the rich tunability of its properties with alloying and strain[10–12] and flexibility in fabrication[13] that make it a promising candidate for device application.[14]

In the bulk, the MIT of VO$_2$ is accompanied by a large structural distortion that has added to the difficulties in unraveling its origins. The high temperature metallic phase resides in the tetragonal rutile structure (isostructural with TiO$_2$). Below the first-order transition temperature, V-V dimers form, accompanied by the twisting of the VO$_6$ octahedra, as the structure is distorted into the insulating monoclinic M_1 phase. A second insulating monoclinic structure (M_2), in which one-half of the V atoms dimerize, is accessible through Cr doping[10] and strain.[12] On the one hand, the dimerization has been considered a hallmark of the Peierls transition, in which the rearrangement of the lattice plays the key role. On the other hand, several experiments have made it clear that electron-electron correlations cannot be ignored,[15]

and should be considered on at least an equal footing.[16]

We report the direct observation of the structural and electronic components of the transition in strained VO$_2$ by *simultaneously* combining powerful spatial and energy resolved probes of the crystal and electronic structure. We further show that the recently-observed monoclinic metallic phase is accessible in the ground state of strained VO$_2$ at ambient temperatures and pressures.

High quality 110 nm thin films of VO$_2$ (r.m.s. roughness of 0.17 nm) were grown on (110)-oriented substrates of rutile TiO$_2$, as described previously,[17] and are hereafter referred to as VO$_2$(110). Electron and photoelectron spectroscopy measurements were performed at the SPELEEM endstation of Beamline I311, MAX-lab (Lund, Sweden), and the samples were prepared for ultrahigh vacuum measurements as described previously.[18,19] Low-energy electron diffraction (LEED) patterns were collected from a 5 μm diameter region of the sample, with the electron emission current restricted to less than 10 nA to minimize radiation damage. Low-energy electron microscopy (LEEM) images were corrected for the non-uniform detector efficiency and background before histogramming; raw images are shown in Fig. 1, and following correction in Fig. 2(a).

Bright-field LEEM images of the surface of VO$_2$(110) are shown in Fig. 1, recorded at an electron energy of 10 eV across the MIT. In this regime, the contrast of LEEM originates from differences in the $(0,0)$ diffraction intensity within the first few atomic layers,[20] and probes the local crystal structure of VO$_2$. LEED patterns (Fig. 1) were also recorded both above and below the transition and confirm the evolution in the crystal structure across the MIT. Above the transition, the LEED pattern at 145 eV resembles the familiar rutile pattern,[21] but at 34 °C additional superstructure spots are visible due to the lower symmetry of the $(110)_R$ monoclinic surface. These measurements also revealed a strong and re-
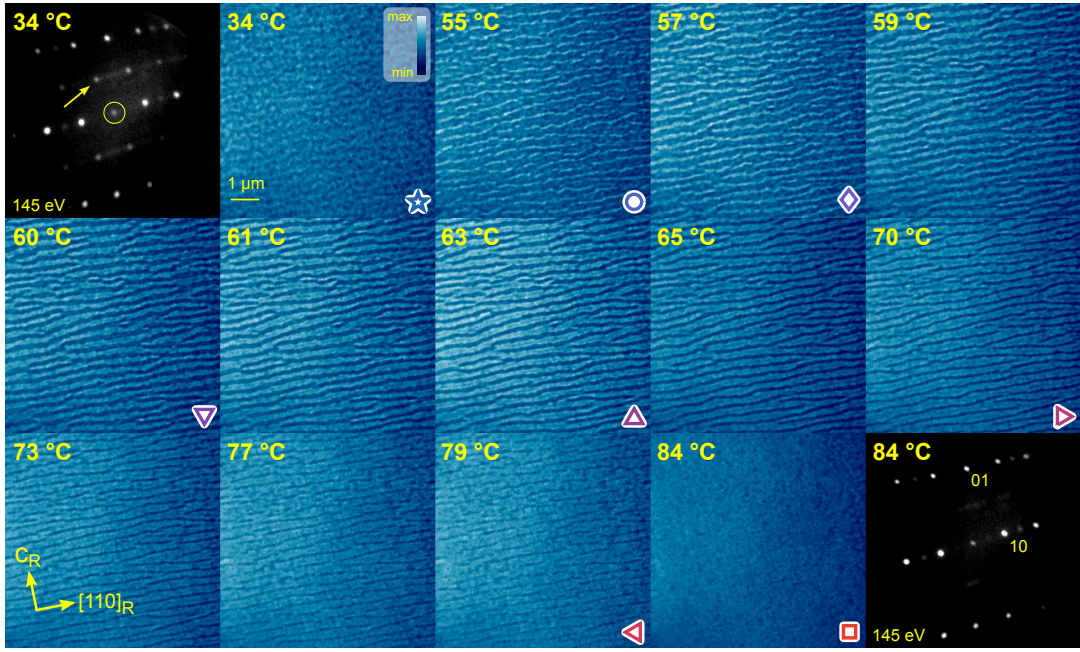
FIG. 1: (Color online) Sequence of LEEM images of VO$_2$(110) recorded at 10 eV. The symbols correspond to the simultaneous acquisition of a PES spectrum [see Fig. 3(a)]. LEED patterns at both endpoints are also shown; the $(0,0)$ spot is circled, and the arrow indicates the extra reflections in the low-symmetry monoclinic phase.

producible sensitivity of the sample surface to both electron and photon irradiation. We emphasize that in all subsequent measurements care was taken to minimize the radiation damage. In particular, exposure to the photon flux was limited to less than 1 min per spectrum, with LEED patterns checked before and after the measurements.

In the monoclinic insulating phase at 34 °C, the LEEM image exhibits a slightly rough appearance, anticipating the emergence of the rutile stripes. At 55 °C, thin stripes of higher LEEM intensity become clearly visible, oriented along the rutile $[110]_R$ crystal direction, in agreement with the previous atomic force microscopy (AFM) and infrared images.[2] These (bright) domains represent regions of the sample with a different crystallographic structure to the insulating monoclinic phase, and can be associated with the transition to the rutile (metallic) phase. As the temperature is increased, the rutile stripes rapidly grow in size until ≈ 65 °C, after which there is a more gradual growth until the stripe structure disappears at 82 °C and the system is fully rutile.

The phase separation between monoclinic and rutile structures we observe in LEEM is reinforced by x-ray photoemission electron microscopy (XPEEM) measurements of the onset of secondary electrons, which provides direct spatial information on the work function of the surface. From photoemission spectroscopy (PES) measurements of the low and high temperature phases, we find that the work function of rutile VO$_2$(110) is 0.12 eV larger than monoclinic VO$_2$(110), in good agreement with recent Kelvin force probe measurements,[22] although opposite to previous PES results on VO$_2$ "nano-bundles".[23] Since the work function is a property of the material surface, and in particular the packing density, it offers an alternative (electronic) perspective to LEEM of the lattice structure. Figures 2(a) and 2(b) show LEEM and XPEEM images respectively of the mixed phase of VO$_2$(110) at 56 °C on the same part of the sample. Since the work function of rutile VO$_2$ is larger than that of monoclinic VO$_2$, the XPEEM contrast is inverted with respect to LEEM, and for clarity the color scale in Fig. 2(b) has been reversed compared to (a). The similarity in the structure between the two images is clear: in addition to the rutile stripes observed in XPEEM, it is possible to identify the same forks in this pattern in both images, e.g. at $(x, y) = (3.3, 2.0)$ μm and $(1.0, 2.0)$ μm. In Fig. 2(c), the XPEEM intensity has been mapped as color onto the LEEM intensity, which is shown as a 2D surface, providing a direct visualization of the spatial correlation between the two probes of the lattice structure: diffraction and work function (electronic).

In Fig. 2(d), the autocorrelation of the LEEM (i.e. $I_{\text{LEEM}} \star I_{\text{LEEM}}$) and XPEEM images is shown along the c_R direction (perpendicular to the rutile stripes). Both functions exhibit a strong, damped cosinusoidal form of the same periodicity, typical of a regularly ordered pattern. Also shown in Fig. 2(d) is the (inverted) cross-correlation between LEEM and XPEEM, $I_{\text{LEEM}} \star I_{\text{XPEEM}}$, which has the same form as the autocorrelation curves, and persists over remarkably long lengthscales. The first peak in the autocorrelation, labeled λ_1 in Fig. 2(d), corresponds to the mean distance
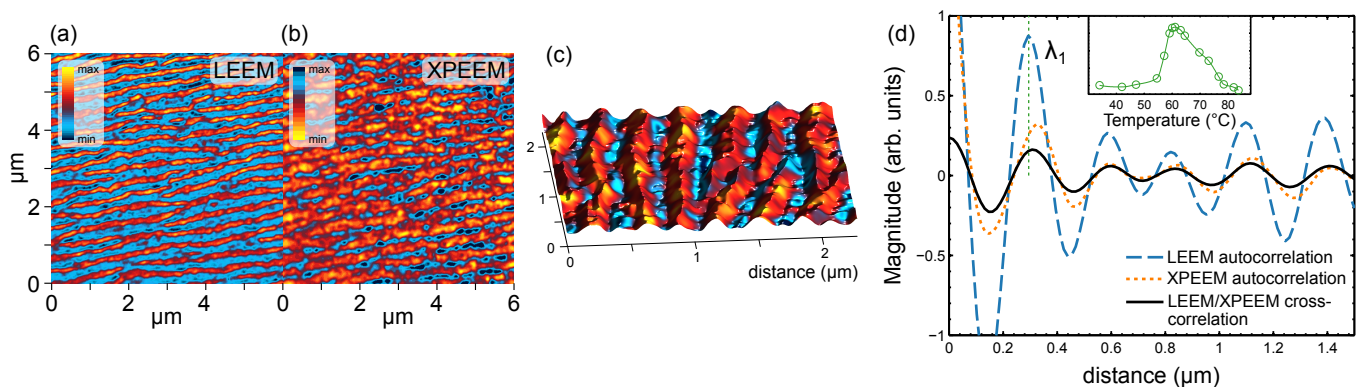
FIG. 2: (Color online) Correspondence between LEEM and XPEEM images, recorded at 56 °C. (a) LEEM image at 10 eV, and (b) XPEEM image of the spatially resolved work function at a photon energy of 50 eV. In (c), the XPEEM intensity in (b) is mapped as false color onto the surface of the LEEM intensity in (a). (d) Autocorrelation of the LEEM and XPEEM images perpendicular to the stripe direction, shown alongside their cross-correlation. λ_1 indicates the location of the first peak in the autocorrelation of the LEEM intensity, and the temperature dependence of its magnitude is shown in the inset.

between stripes, and is $\approx$ 300 nm. The temperature dependence of the magnitude of this peak is shown in the inset to Fig. 2(d). The rapid rise above 55 °C corresponds to the stripe formation, and the shoulder at 70 °C reflects their more gradual growth towards the end of the transition. The strong quantitative correlation between LEEM and XPEEM illustrates the structural nature of the stripe pattern, in agreement with the topographic rumpling of the surface previously observed via AFM.[2]

We now turn to PES to directly explore the electronic behavior of the stripes. At selected temperatures through the MIT, PES spectra were simultaneously recorded (within 1 min of the corresponding LEEM image) at a photon energy of 50 eV, and are shown in Fig. 3(a). The PES spectra are composed of O $2p$ states between 36 and 43 eV, and V $3d$ states near the Fermi level above 43 eV, and are qualitatively similar to previous PES measurements.[19,24,25] Below the MIT (bottom spectrum), the V $3d$ states are relatively narrow, whereas above the transition the transfer of spectral weight into quasiparticle states at the Fermi level (higher kinetic energies) indicates the formation of the metallic phase. The top inset to Fig. 3(a) shows the evolution in the leading edge of the V $3d$ states with temperature, determined by locating the extrema in the derivative of the PES. This quantity is found to shift to higher energies by 0.19 eV over the measured temperature range, and is in good agreement with high-resolution dichroic PES measurements.[19]

The LEEM and PES results are compared in Fig. 3(b) by analyzing the fractions of their constituent components with temperature. At the energies employed in this study, both LEEM and PES (and, indeed, LEED) have similar depth sensitivities (of $\lesssim$ 1 nm), meaning our results probe essentially the same physical volume of the sample. Histograms were constructed of the intensity of each LEEM image in Fig. 1, which were fitted to either one or two Gaussian components (below 47 °C only

a single component could be resolved). For the other images, the fraction of the brighter component was associated with the rutile phase [as shown in Fig. 3(c)], and the results are shown by the squares in Fig. 3(b). Correspondingly, the fraction of the metallic phase has been estimated from the PES data by assuming the endpoints (at 34 °C and 86 °C) are representative of each phase. The intermediate spectra have been fitted to a linear combination of these two end-points (see Ref. 19 for an example of this procedure), and the results are shown by the circles in Fig. 3(b). We emphasize that we do not find evidence of a third component in either LEEM or PES analyses, although we cannot rule out such a phase below our detection level. The plateau in the progression of the MIT discussed above is clearly evident in both LEEM and PES data between 65 °C and 75 °C in Fig. 3(b), and may be related to the interface energy of the stripe domains.

The good qualitative agreement in Fig. 3(b) is mitigated slightly by the higher fraction of the metallic phase extracted from the PES data. To gain additional insight, we have repeated this procedure focusing separately on the O $2p$ and V $3d$ states by restricting the regions-of-interest of the fit [shown in the inset to Fig. 3(b)]. Remarkably, the metallic fraction determined from the O $2p$ states alone is found to closely follow that determined from LEEM. Since the O $2p$ states are most sensitive to their bonding environment (i.e. the structure of the material), this provides a satisfying quantitative link between LEEM and PES. On the other hand, the metallic fraction determined from the V $3d$ states shows quite different behavior: it initially rapidly rises before saturating near 60 °C, strongly reminiscent of the temperature evolution of the leading edge of the PES shown in Fig. 3(a). A specific example is shown in Fig. 3(c-e), in which the histogram of the LEEM intensity at 59 °C (c) clearly shows two components of approximately the same area (the metallic fraction is determined to be 50%). How-
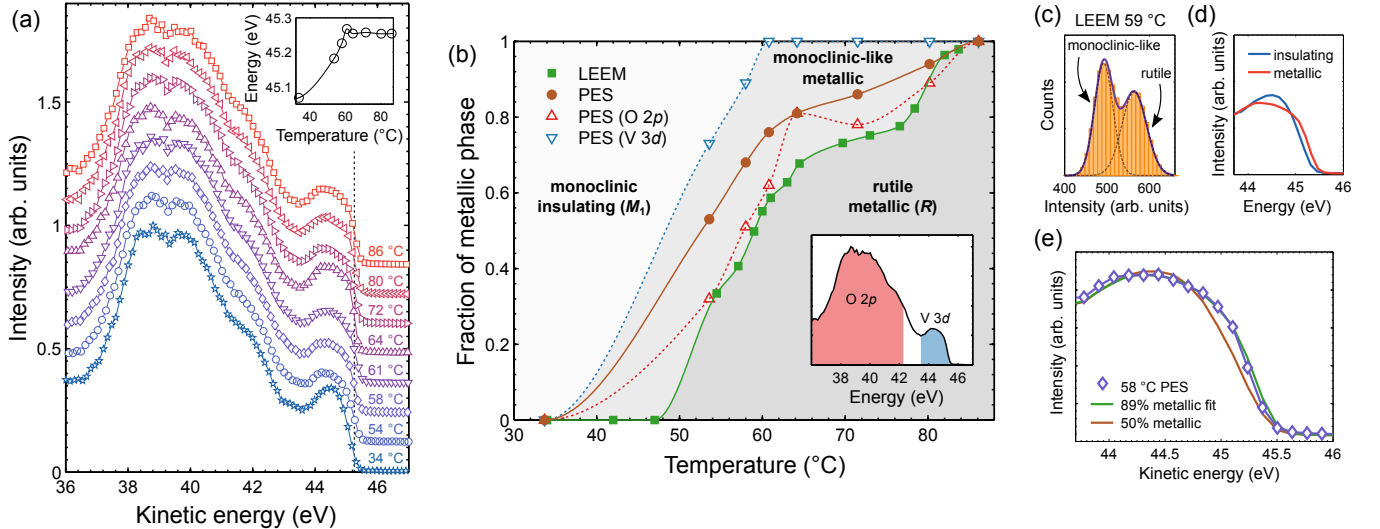
FIG. 3: (Color online) (a) PES measurements of $VO_2(110)$ across the MIT recorded on the same part of the sample as the LEEM images of Fig. 1. The upper inset illustrates the evolution of the leading edge of the spectra with temperature. (b) The fraction of the metallic phase extracted from LEEM and PES (the lines are guides for the eye). The inset shows the regions-of-interest used for the separate analysis of O 2p and V 3d states. (c) Histogram of the LEEM intensity at 59 °C. (d) Magnified view of the V 3d states in the insulating and metallic phases. (e) Results of fitting the insulating and metallic end-points to the 58 °C PES data in the V 3d region (89% metallic fraction). The spectrum corresponding to the LEEM results (50% metallic fraction) is also shown for comparison.

ever, the V 3d spectrum at this temperature (e) cannot be described as a 50:50 average of the insulating and metallic end-points (d). Instead, it is well approximated if a metallic fraction of 89% is assumed (e). A previous nanoscale imaging study, combining structural (diffraction) and electronic (infrared scattering) probes, also noticed differences in the progression of the structural and electronic components in VO_2 thin films,[26] although we do not observe the non-monotonic evolution in the structure reported by those authors.

Taken together, these results reveal a separation of the temperature scales of the structural and electronic transitions in $VO_2(110)$, the former of which is not complete until ~ 84 °C whereas the latter becomes fully metallic (within our precision) at ≈ 61 °C. At intermediate temperatures (60 – 80 °C) $VO_2(110)$ consists of a mixture of rutile metallic and monoclinic-like metallic phases, where we use the qualifier "like" to indicate the LEEM intensity and O 2p photoelectrons closely resemble the monoclinic M_1 phase. At lower temperatures (50 – 60 °C) all three phases are in equilibrium. Such monoclinic metallic states in VO_2 have previously been identified under high pressure[4,5] and in out-of-equilibrium measurements (e.g. photoexcited pump-probe, charge-doped or voltage-driven experiments).[6] In our strained $VO_2(110)$ film, the a and b lattice parameters (determined from x-ray diffraction) correspond to a compressive strain along the [110] axis of $\sim 2\%$, which corresponds to approximately 12 GPa of hydrostatic pressure, very close to the onset of the monoclinic metallic phase in high-pressure measurements.[27] Our results reveal that this unusual new

phase is accessible *in the ground state* at ambient temperatures and pressures in epitaxially strained VO_2.

The full structural and electronic details of monoclinic-like metallic phase(s) in VO_2 have yet to be experimentally reported, although there are already several hints. For example, detailed structural measurements of bulk VO_2, accompanied by band structure calculations, suggest the melting of the V-V dimers may stabilize the metallic state before the tetragonal symmetry is adopted,[28] a picture that is supported by first-principles calculations of the photoinduced transition.[29] At high pressure, Raman measurements indicate a rearrangement of the V-V dimers.[4]

Given the available information, it is possible that the monoclinic-like metallic phase that we observe develops due to the spontaneous breaking, or substantial weakening, of the V-V bond, while the system remains monoclinic, and this phase is stabilized by the high in-plane effective pressure due to the substrate clamping. Alternatively, if the V-V dimers remain strongly paired in this phase, electron-electron correlations may drive the transition. It is therefore likely that the structural details in this phase are capable of distinguishing the dominant interaction that drives the MIT. Ultimately, given the possible proximity of VO_2 to a conventional Mott-Hubbard transition,[19,30] coupled with the several structural instabilities accessible through pressure and chemical doping,[1,10,31] it may turn out that the photoinduced and thermodynamic monoclinic metallic phases differ. Future planned measurements are required to clarify the fate of the V-V dimers in the monoclinic-like metallic

phase, which may finally hold the key to a deeper understanding of the microscopic mechanism of the MIT in VO_2.

[1] J. H. Park, J. M. Coy, T. S. Kasirga, C. Huang, Z. Fei, S. Hunter and D. H. Cobden, Nature (London) **500**, 431 (2013).

[2] M. K. Liu, M. Wagner, E. Abreu, S. Kittiwatanakul, A. McLeod, Z. Fei, M. Goldflam, S. Dai, M. M. Fogler, J. Lu, S. A. Wolf, R. D. Averitt, D. N. Basov, Phys. Rev. Lett. **111** 096602 (2013).

[3] M. K. Liu, M. Wagner, J. Zhang, A. McLeod, S. Kittiwatanakul, Z. Fei, E. Abreu, M. Goldflam, A. J. Sternbach, S. Dai, K. G. West, J. Lu, S. A. Wolf, R. D. Averitt and D. N. Basov, Appl. Phys. Lett. **104**, 121905 (2014).

[4] E. Arcangeletti, L. Baldassarre, D. Di Castro, S. Lupi, L. Malavasi, C. Marini, A. Perucchi and P. Postorino, Phys. Rev. Lett. **98**, 196406 (2007).

[5] W.-P. Hsieh, M. Trigo, D. A. Reis, G. A. Artioli, L. Malavasi and W. L. Mao, Appl. Phys. Lett. **104**, 021917 (2014).

[6] H.-T. Kim, Y. W. Lee, B.-J. Kim, B.-G. Chae, S. J. Yun, K.-Y. Kang, K.-J. Han, K.-J. Yee and Y.-S. Lim, Phys. Rev. Lett. **97**, 266401 (2006); B.-J. Kim, Y. W. Lee, S. Choi, J.-W. Lim, S. J. Yun, H.-T. Kim, T.-J. Shin and H.-S. Yun, Phys. Rev. B **77**, 235401 (2008); Z. Tao, T.-R. T. Han, S. D. Mahanti, P. M. Duxbury, F. Yuan, C.-Y. Ruan, K. Wang and J. Wu, Phys. Rev. Lett. **109**, 166406 (2012); T. L. Cocker, L. V. Titova, S. Fourmaux, G. Holloway, H.-C. Bandulet, D. Brassard, J.-C. Kieffer, M. A. El Khakani and F. A. Hegmann, Phys. Rev. B **85**, 155120 (2012).

[7] Y. Ding, C.-C. Chen, Q. Zeng, H.-S. Kim, M. J. Han, M. Balasubramanian, R. Gordon, F. Li, L. Bai, D. Popov, S. M. Heald, T. Gog, H.-K. Mao and M. van Veenendaal, Phys. Rev. Lett. **112**, 056401 (2014).

[8] F. J. Morin, Phys. Rev. Lett. **3**, 34 (1959); N. F. Mott, *Metal-Insulator Transitions*, Taylor & Francis Ltd, London (1974).

[9] A. Cavalleri, Cs. Tóth, C. W. Siders, J. A. Squier, F. Ráksi, P. Forget and J. C. Kieffer, Phys. Rev. Lett. **87**, 237401 (2001).

[10] J. P. Pouget, H. Launois, T. M. Rice, P. Dernier, A. Gossard, G. Villeneuve and P. Hagenmuller, Phys. Rev. B **10**, 1801 (1974).

[11] G. Villeneuve, A. Bordet, A. Casalot, J. P. Pouget, H. Launois and P. Lederer, J. Phys. Chem. Solids **33**, 1953 (1972).

[12] J. P. Pouget, H. Launois, J. P. D'Haenens, P. Merenda and T. M. Rice, Phys. Rev. Lett. **35**, 873 (1975).

[13] Y. Muraoka and Z. Hiroi, Appl. Phys. Lett. **80**, 583 (2002); J. Cao, E. Ertekin, V. Srinivasan, W. Fan, S. Huang, H. Zheng, J. W. L. Yim, D. R. Khanal, D. F. Ogletree, J. C. Grossman and J. Wu, Nature Nanotech. **4**, 732 (2009).

[14] K. Appavoo, B. Wang, N. F. Brady, M. Seo, J. Nag, R. P. Prasankumar, D. J. Hilton, S. T. Pantelides and R. F. Haglund, Jr., Nano Lett. **14**, 1127 (2014).

[15] A. Zylbersztejn and N. F. Mott, Phys. Rev. B **11** 4383 (1975).

[16] M. W. Haverkort, Z. Hu, A. Tanaka, W. Reichelt, S. V. Streltsov, M. A. Korotin, V. I. Anisimov, H. H. Hsieh, H.-J. Lin, C. T. Chen, D. I. Khomskii and L. H. Tjeng, Phys. Rev. Lett. **95**, 196404 (2005).

[17] K. G. West, J. W. Lu, J. Yu, D. Kirkwood, W. Chen, Y. H. Pei, J. Claassen and S. A. Wolf, J. Vac. Sci. Technol. A **26**, 133 (2008); S. Kittiwatanakul, J. Laverock, D. Newby, Jr., K. E. Smith, S. A. Wolf and J. Lu, J. Appl. Phys. **114**, 053703 (2013).

[18] J. Laverock, L. F. J. Piper, A. R. H. Preston, B. Chen, J. McNulty, K. E. Smith, S. Kittiwatanakul, J. W. Lu, S. A. Wolf, P.-A. Glans and J.-H. Guo, Phys. Rev. B **85**, 081104(R) (2012).

[19] J. Laverock, A. R. H. Preston, D. Newby, Jr., K. E. Smith, S. Sallis, L. F. J. Piper, S. Kittiwatanakul, J. W. Lu, S. A. Wolf, M. Leandersson and T. Balasubramanian, Phys. Rev. B **86**, 195124 (2012).

[20] E. Bauer, Rep. Prog. Phys. **57**, 895 (1994).

[21] E. Goering, M. Schramme, O. Müller, R. Barth, H. Paulin, M. Klemm, M. L. denBoer and S. Horn, Phys. Rev. B **55**, 4225 (1997).

[22] C. Ko, Z. Yang and S. Ramanathan, ACS Appl. Mater. Interfaces **3**, 3396 (2011).

[23] H. Yin, M. Luo, K. Yu, Y. Gao, R. Huang, Z. Zhang, M. Zeng, C. Cao and Z. Zhu, ACS Appl. Mater. Interfaces **3**, 2057 (2011).

[24] K. Okazaki, H. Wadati, A. Fujimori, M. Onoda, Y. Muraoka and Z. Hiroi, Phys. Rev. B **69**, 165104 (2004); K. Saeki, T. Wakita, Y. Muraoka, M. Hirai, T. Yokoya, R. Eguchi and S. Shin, Phys. Rev. B **80**, 125406 (2009).

[25] T. C. Koethe, Z. Hu, M. W. Haverkort, C. Schüßler-Langeheine, F. Venturini, N. B. Brookes, O. Tjernberg, W. Reichelt, H. H. Hsieh, H.-J. Lin, C. T. Chen and L. H. Tjeng, Phys. Rev. Lett. **97**, 116402 (2006); R. Eguchi, M. Taguchi, M. Matsunami, K. Horiba, K. Yamamoto, Y. Ishida, A. Chainani, Y. Takata, M. Yabashi, D. Miwa, Y. Nishino, K. Tamasaku, T. Ishikawa, Y. Senba, H. Ohashi, Y. Muraoka, Z. Hiroi and S. Shin, Phys. Rev. B **78**, 075115 (2008).

[26] M. M. Qazilbash, A. Tripathi, A. A. Schafgans, B.-J. Kim, H.-T. Kim, Z. Cai, M. V. Holt, J. M. Maser, F. Keilmann, O. G. Shpyrko and D. N. Basov, Phys. Rev. B **83**, 165108 (2011).

[27] M. Mitrano, B. Maroni, C. Marini, M. Hanfland, B. Joseph, P. Postorino and L. Malavasi, Phys. Rev. B **85**, 184108 (2012).

[28] T. Yao, X. Zhang, Z. Sun, S. Liu, Y. Huang, Y. Xie, C. Wu, X. Yuan, W. Zhang, Z. Wu, G. Pan, F. Hu, L. Wu, Q. Liu and S. Wei, Phys. Rev. Lett. **105**, 226405 (2010).

[29] X. Yuan, W. Zhang and P. Zhang, Phys. Rev. B **88**, 035119 (2013); M. van Veenendaal, Phys. Rev. B **87**, 235118 (2013).

[30] B. Lazarovits, K. Kim, K. Haule and G. Kotliar, Phys. Rev. B **81**, 115117 (2010).

[31] J. B. Goodenough and H. Y.-P. Hong, Phys. Rev. B **8**, 1323 (1973).